Charge localization, stabilization and hopping in lead-halide perovskites: Competition between polaron stabilization and cation disorder

Francesco Ambrosio,[a,b,*] Daniele Meggiolaro,[a,b] Edoardo Mosconi, [a,b] Filippo De Angelis[a,b,c*]

[a]*Computational Laboratory for Hybrid/Organic Photovoltaics (CLHYO), Istituto CNR di Scienze e Tecnologie Molecolari (ISTM-CNR), Via Elce di Sotto 8, 06123 Perugia, Italy*

[b]*CompuNet, Istituto Italiano di Tecnologia, Via Morego 30, 16163 Genova, Italy*

[c]*Department of Chemistry, Biology and Biotechnology, University of Perugia, Via Elce di Sotto 8, 06123 Perugia, Italy*

*E-mail: Francesco.Ambrosio@iit.it, filippo@thch.unipg.it

Abstract

Metal halide perovskites, of general formula ABX_3, show a complex interplay of the inorganic BX_3 sub-lattice and the organic/inorganic A-site cations, which likely determines some of their peculiar optoelectronic properties. Comprehension of the physics underlying this interaction may reveal further means of fine-tuning their optoelectronic response. Here, we investigate in depth charge/lattice interactions associated to the formation of polarons in different models of the prototypical $CH_3NH_3PbI_3$ perovskite through advanced electronic-structure calculations. We demonstrate that charge localization, while induced by the disordered dipolar field of the organic cations, is only stabilized by distortions in the inorganic sub-lattice. Polaron hopping between neighbouring minima is related to the random reorientation of the organic cations and occurs via a delocalized transition state. Our simulations highlight a struggle between thermally induced disorder, driven by the motion of A-site cations, and polaron stabilization within the BX_3 sub-lattice, which explains the simultaneous low mobility and high diffusion length of charge carriers in lead-halide perovskites.

TOC graphics

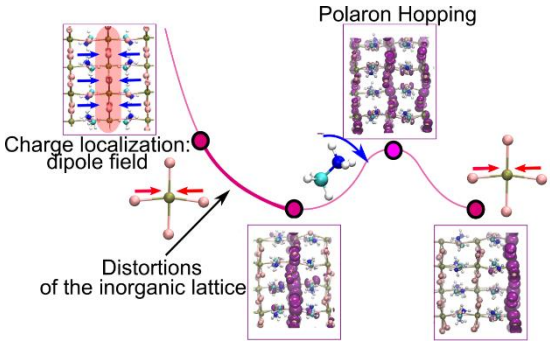

Metal halide perovskites have represented a major breakthrough in photovoltaics, with efficiencies rivalling those of established silicon-based solar cells.[1-3] The electronic and optical properties of this class of materials are intriguing and puzzling *at the same time*, thus motivating the large efforts devoted to explain them.[4-16] For example, while the recombination of photogenerated carriers is as slow as those measured for the best inorganic crystalline materials such as GaAs,[11-15, 17] the mobility of these carriers is indeed modest. [18]

The slow bimolecular recombination between electrons and holes in the archetypal methylammonium lead iodide perovskite, $CH_3NH_3PbI_3$, is an intrinsic property for which different explanations have been proposed. Early studies have suggested a key role of the organic cations in either (i) determining a different nanoscale localization of the valence and the conduction band-edge states[19, 20] or (ii) contributing to an exciton screening mechanism.[21, 22] More recently, a different interpretation of this phenomenon has been proposed, based on polaron formation.[23-28] In this context, the role of the organic cation has been somehow scaled down. In fact, measurements have shown that (i) polaron formation occurs on the sub-picosecond timescale,[29, 30] thus being much faster than the rotation of the organic cations,[31, 32] which takes place on a several picoseconds time scale; and (ii) bimolecular recombination coefficients for $CsPbI_3$ are comparable to those of related perovskites bearing organic cations.[33] In line with this picture, first-principles molecular dynamics simulations of the fully inorganic $CsPbI_3$ revealed the occurrence of a disordered A-site cation environment similar to that observed in $CH_3NH_3PbI_3$.[34, 35] Simulations have also shown that, upon photoexcitation, electrons and holes become spatially separated.[4] Such a separate localization reconciles the measured low recombination rates with the polaronic nature of the charge carriers.[23, 36] In fact, previous measurements and calculations of phonon dispersion have suggested that recombination in hybrid lead halide perovskites follows a classic band-structure picture for polar inorganic semiconductors (*e.g.* GaAs).[36, 37] Theoretical models based on band-to-band transitions has been used to calculate bimolecular recombination rates in excellent agreement with the experiment,[36] a result which would be dramatically altered by the inclusion of polarons.[23]

However, the increased effective mass of polaronic charge carriers, that should favour recombination, is compensated by the lowered overlap of the charge carriers.[4] The spatial separation of polarons has been recently invoked also as a possible cause to reduced recombination at defects.[38]

Charge localization is found to be mainly induced by the structural reorganization of the inorganic sub-lattice, with a limited contribution of the dipolar field associated with the organic cations, in both first-principle simulations and tight-binding models.[4, 39] However, recent experiments have highlighted a remarkable correlation between the diffusion length of charge carriers and the rotational time of organic cations within the inorganic cage. In particular, $CH(NH_2)_2PbI_3$, bearing the faster-rotating formamidinium cation, exhibits a significantly longer diffusion length of charge carriers than $CH_3NH_3PbI_3$,[32, 40] thus motivating a renewed interest towards the role of the A-site cations in the physics of metal-halide perovskites.

The low mobility of charge carriers in perovskites has been recently related to the properties of large polarons distributed over several unit cells.[41] In particular, large-scale atomistic simulations suggested that polaron hopping is induced by the dynamic disorder of the organic cations in $CH_3NH_3PbI_3$. Furthermore, the interplay between the vibrations of the inorganic lattice and the random rotation of the organic cations was estimated to approximately half the mobility of charge carriers.[41] Alternatively, a model based on *ab initio* calculations correlated the poor mobility of charge carriers in $CH_3NH_3PbI_3$ with the low frequencies of Pb-I vibrations, and therefore the high thermal activation of phonons.[42] However, hole and electron polarons were found to hop from one localization site to another on a sub-picosecond time-scale in molecular dynamics simulations, a result apparently contrasting with the low mobility usually associated with charge carriers in metal-halide perovskites.[4, 38]

Overall, while significant progress has been achieved in the study of the optoelectronic properties of this class of materials, there are still fundamental questions that remain unanswered. In particular, while the occurrence of polarons in $CH_3NH_3PbI_3$ and other lead-halide perovskites has

been demonstrated by both theory and experiments,[4, 29, 43] the distinct role and the complex interplay between the inorganic sub-lattice and the A-site cations, whether organic or not, still eludes a comprehensive characterization. In fact, even if distortions in the inorganic sub-lattice stabilize the localized charge, such a localization might be inaccessible in absence of a disordered dipole field generated by the A-site cations. Furthermore, the mechanism by which these polarons move from site to site in the material is still unclear: once a structural distortion has stabilized the polaron in a region of the inorganic sub-lattice, how this quasi-particle escapes from this local minimum and what is the role of the randomly oriented cations remain to be clarified.

In this Letter, we quantitatively discern the contributions to charge localization and stabilization due to the inorganic lattice and the organic cations in the prototypical $CH_3NH_3PbI_3$ perovskite. In particular, we perform Density Functional Theory (DFT) calculations on a set of structural models with a different orientation of the organic cations. Our results indicate that, while charge localization is indeed thoroughly correlated to the orientation of the organic cations, stabilization is mainly attained by local distortions in the inorganic sub-lattice. Considering that the organic cations themselves are only marginally influenced by the presence of charges, this suggests that polaron formation in lead halide perovskites is guided by the chaotic and disordered dipolar field generated by the A-site cations, which may favour localization in a given region of the material. We calculate energy barriers of 150 and 80 meV for hole and electron polaron hopping in adjacent localization sites, respectively. These values (i) are comparable to the calculated stabilization energy of the polarons, with hopping being accomplished by a charge-delocalized transition state, and (ii) lead to drastically lower hopping frequencies than those observed in molecular dynamics simulations. Recalculation of the energy barriers in absence of A-site cations suggests their key role in the hopping mechanism, thus explaining both the correlation between diffusion lengths and rotation times and the low mobility of charge carriers experimentally measured.

We carry out hybrid DFT calculations by employing the PBE0 functional[44, 45] for different structural models of tetragonal $CH_3NH_3PbI_3$. The fraction of Fock exchange α is kept fixed at its original value (0.25), since it has been found to comply with the Koopmans' condition.[46] This ensures that the calculations are not biased by the self-interaction error,[4,47, 48] which would alter the energetics of the system [(cf. Supplementary Information (SI) for the calculation of the polaron binding energy]. We include non-local van der Waals interactions through the rVV10 scheme.[49, 50] All calculations are carried out with the freely-available CP2K suite of codes.[51] Goedecker-Teter-Hutter pseudopotentials are used to account for core-valence interactions.[52] We use double-ζ polarized basis sets for the wave functions[53] and a cut-off of 300 Ry for the expansion of the electron density in plane waves. We employ the auxiliary density matrix method to speed up the calculation of exact exchange in hybrid functional calculations as implemented in CP2K with the cFIT auxiliary basis set.[54] Calculations are performed on different structural configurations of a 384-atoms 2×2×2 supercell with lattice parameters $a = b = 17.72$ Å, $c = 25.32$ Å, corresponding to the experimental structure.[55] The results achieved with this computational setup have been benchmarked against calculations performed on larger supercells, as reported in the SI.

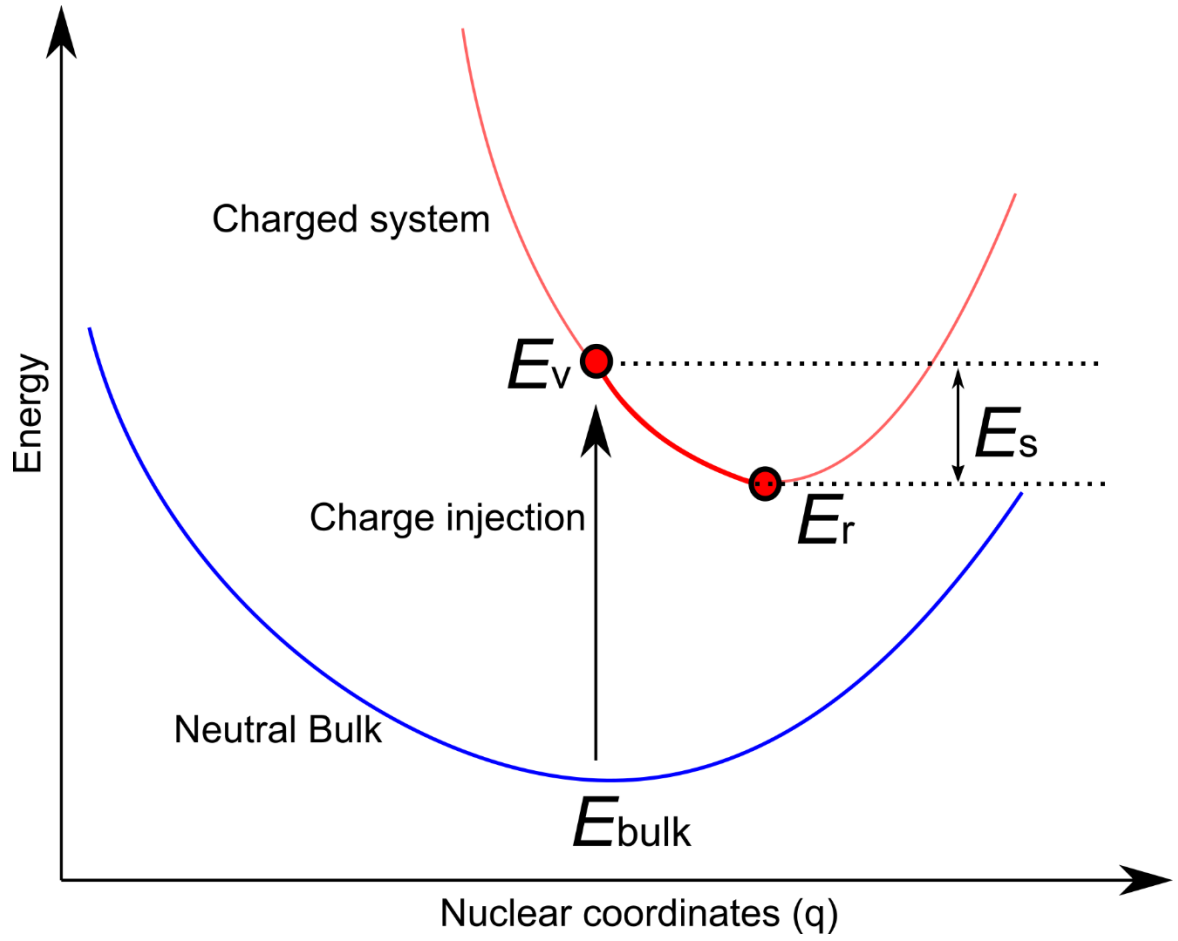

Scheme 1. Schematic representation of the stabilization energy of polarons, as defined in the main text.

We first aim at describing the nature of the localization and of the stabilization of hole and electron polarons in $CH_3NH_3PbI_3$. To this end, we perform structural relaxations in the presence of an extra positive or negative charge and. For each system, we calculate the stabilization energy, defined as follows: $E_s^{\pm} = E_v^{\pm 1} - E_r^{\pm 1}$, where $E_v^{\pm 1}$ is the total energy of the supercell upon vertical injection of the positive or negative charge into the neutral system and $E_r^{\pm 1}$ is the total energy of the charged supercell, upon structural relaxation. Electrostatic finite-size effects appearing for calculations of charged periodic supercells are here neglected due to the large dielectric constant of $CH_3NH_3PbI_3$.[56] The calculated quantities are schematized in Scheme 1.

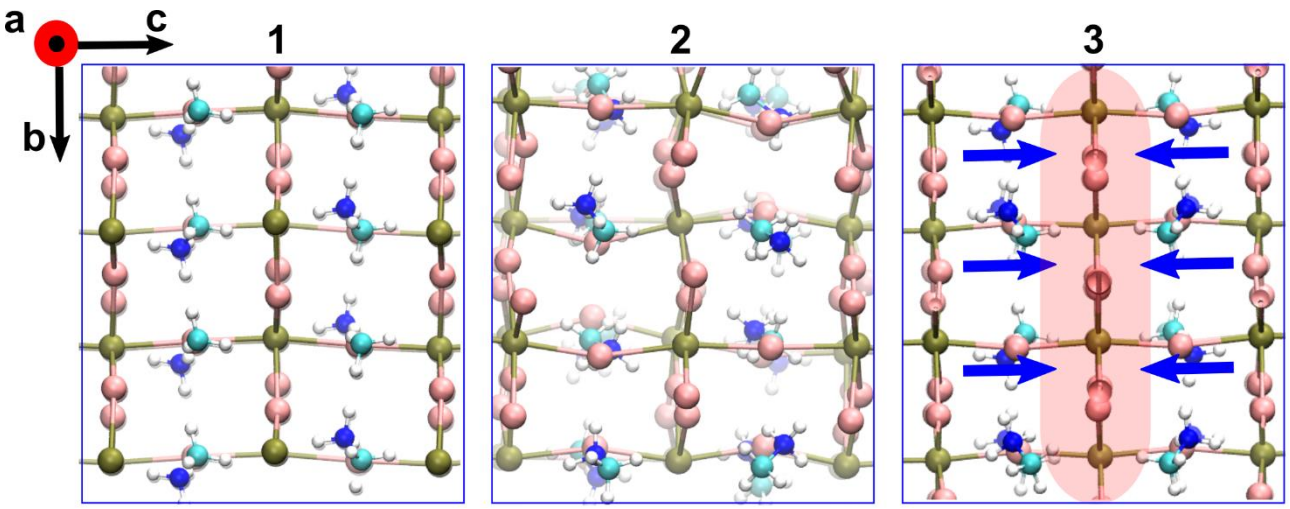

Figure 1. Models of tetragonal $CH_3NH_3PbI_3$ employed in this work. Pb atom in grey, I in pink, N in blue, C in cyan, and H in white. The tetragonal axis lies horizontally. For model **3**, the Pb-I plane in which localization of the hole is favoured has been shaded.

We calculate the stabilization energy, $E_s^{\pm}$, from three different structural models:

(i) the most stable structural model of tetragonal $CH_3NH_3PbI_3$, **1** in Fig. 1.[57] This model reasonably represents the tetragonal structure of $CH_3NH_3PbI_3$ at low temperature, but above the phase transition to the orthorhombic phase;

(ii) structural configurations extracted from *ab initio* molecular dynamics (AIMD) simulations with extra holes and electrons, **2** in Fig. 1. These provide us with a reliable model of hole and electron polarons at room temperature, thus including both the disorder induced by the rotation of the cations and thermal disorder of the lattice.

(iii) a structural model, **3** in Fig. 1, in which the organic cations are all oriented towards a selected Pb-I plane. This model is built to maximize the dipole field of the A-cations.

A summary of the results is collected in Table 1. For structure **1**, we calculate small stabilization energies for both hole and electron ($E_s^+ = 13$ meV, $E_s^- = 9$ meV). In fact, in absence of a significant dipolar or thermal disorder, charges are found to be delocalized in the respective band-

edge states (cf. Fig. 2). In contrast, structure **2** features larger values for both E_s^+ and E_s^-, which amount to 130 and 90 meV, respectively, as calculated from averages over five different configurations, equally spaced in time by 500 fs, sampled during the AIMD trajectory. In this case, the extra charges are found to be localized forming large polarons. For example, the hole polaron (cf. Fig. 2) localizes on a Pb-I plane, following a distortion of the inorganic lattice in the plane which brings to a contraction of Pb-I bonds, in accord with the antibonding nature of the valence band edge states.[4, 43] The stabilization energy for structure **3**, in which charge separation induced by the dipole field is enhanced by construction, is comparable to those obtained for the AIMD-derived structures, with $E_s^+ = 110$ meV and $E_s^- = 60$ meV. It should be noted that the total energy difference between systems **3** and **1** for the relaxed neutral structures, $\Delta E_r = E_r(3) - E_r(1)$, is 580 meV.[57] Therefore, structure **3** is noticeably less stable than the corresponding structure **1**. This implies that achieving a specifically ordered orientation of the A-site cations is energetically (and entropically) expensive. When adding an extra charge to model **3**, we observe formation of a polaron upon structural relaxation, similarly to that achieved for structure **2** (cf. Fig. 2). The calculated total energy difference between structure **3** and **1** for the positively charged systems, $\Delta E_r^+ = E_r^+(3) - E_r^+(1)$, is 260 meV, a value reduced by 280 meV, compared to ΔE_r.

Table 1. Calculated values of stabilization energies (meV) for hole and electron polarons for different structural models of tetragonal $CH_3NH_3PbI_3$. The value in parenthesis for structure **3** is calculated from structural relaxation of the sole methylammonium cations.

Structure	E_s^+	E_s^-
1	13	9
2	140	90
3	110 (4)	60

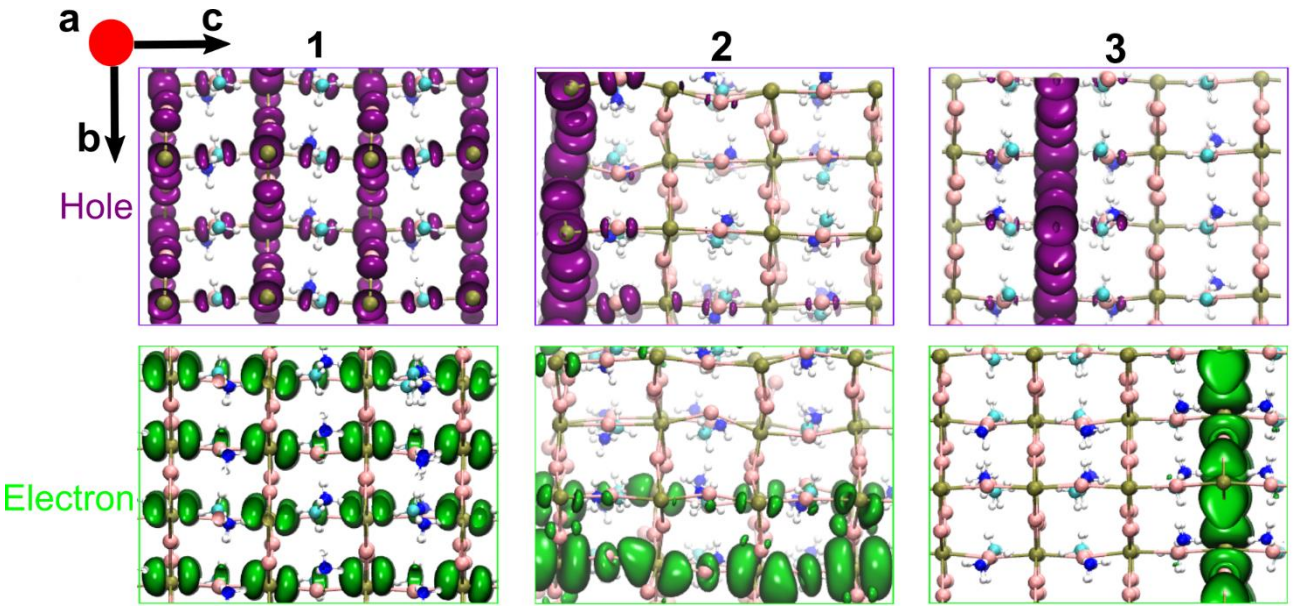

Figure 2. Isodensity representation of the extra hole (in purple) and the extra electron (in green) after structural relaxation for the three models of tetragonal $CH_3NH_3PbI_3$ employed in this work. Pb atom in grey, I in pink, N in blue, C in cyan, and H in white. The tetragonal axis lies horizontally.

In **3**, hole (electron) localizes on the Pb-I plane to which the carbon (nitrogen) atoms of the methylammonium cations are pointing (cf. Fig. 3). This further demonstrates how charge localization is intimately related to the orientation of the organic cations, as previously suggested.[57] In order to verify whether the orientation of the dipole is also sufficient to stabilize the polaron or not, we perform a constrained structural relaxation of the positively charged structure **3**. In this calculation, the atoms belonging to the inorganic sub-lattice are frozen to their position in the respective neutral system and only methylammonium cations are allowed to move. We then recalculate E_s^+, finding a value of 4 meV: polaron stabilization essentially vanishes even for a model system created to emphasize the dipole field of the organic cations. Therefore, the energy gain in polaron formation can be unambiguously attributed to the distortions in the inorganic sub-lattice. Such distortions, however, are found to be clearly guided by the orientation of the

methylammonium cations, thus indicating a synergistic mechanism for polaron formation and stabilization. The dipole field generated by an ordered orientation of cations, as observed in structure **3**, locally pins band edges in the inorganic plane to which the dipoles point. Notably, in structure **3**, the ordered alignment of cations destabilizes the valence band maximum (VBM) of 220 meV in the neutral perovskite compared to structure **1**, leading to a reduction of the band gap. The VBM up-shift observed in structure **3** leads to a local decrease of the ionization potential and to a larger stabilization of the hole polaron compared to structure **1**. This evidence is further confirmed by the comparison of total energies of structures **1** and **3** in their positive charged state when the lattice is frozen at the respective neutral equilibrium geometries, $\Delta E^{+}_{r-\mathrm{MA}} = E^{+}_{r-\mathrm{MA}}(3) - E^{+}_{r-\mathrm{MA}}(1)$. We calculate $\Delta E^{+}_{r-\mathrm{MA}} = 370$ meV to be compared with $\Delta E_r = 580$ meV**.** Therefore, the sole dipole field is found to reduce the energy difference between these two structures by almost 210 meV, a value comparable with the observed energy shift of the VBM in the neutral systems.

Overall, the results of calculations performed on models **1** and **3** clearly indicate that polarons should not form at 0 K. However, structural configurations bearing the dipolar and thermal disorder, which promotes polaron formation, are available at room temperature (model **2**). This physical picture is also consistent with the higher bimolecular recombination rates that have been measured for the orthorhombic phase of $CH_3NH_3PbI_3$[13], stable at low temperature, for which thermal energy is not sufficient to induce disorder in the material.

Next, we describe the hopping mechanism of hole and electron polarons in $MAPbI_3$. It has been previously shown that hole (electron) polarons hop from one localization plane (chain) of Pb-I atoms to another on a sub-picosecond time-scale.[4] This time scale is indeed typical of valence and conduction band edges fluctuation retrieved by AIMD simulations.[20] Here, for both type of polarons we pick the two structural configurations closest in time for which localization of the charge occurs in adjacent sites [cf. Fig. 3 (a)]. For each structure, we perform a structural relaxation in presence of

the charge and we verify that the polaron localization is retained. In this way, thermal effects do not influence the total energies of the two models, which are found to differ by less than 20 meV. Then, we employ a modified version of the linear transit method[58] to construct intermediate structures connecting the two limiting structures along a linear path (cf. SI).

For hole polaron hopping, we estimate an energy barrier of 150±10 meV, considering the average of the values calculated from the two different end points. [cf. Fig. 3 (a)]. This is very close to the calculated value of $E_S^{\pm}$ for the respective models. In fact, inspection of the wave function of the structure corresponding to the energy maximum along the linear path [cf. Fig. 3 (a)] indicates that hopping of the polaron is achieved through a partly delocalized state in which the hole is shared among adjacent Pb-I planes. An energy barrier of 80±10 meV [cf. Fig. 3 (b)] is calculated for electron polaron hopping, a value in accord with the lower stabilization of this polaron in the material and again consistent with a physical picture in which hopping occurs through a semi-delocalized state among adjacent localization sites. It should be noted that spin-orbit coupling (SOC) significantly contributes to the electronic properties of $CH_3NH_3PbI_3$.[7, 10] On this regard, the effect induced by SOC on valence band-edge state is rather limited,[59] ensuring that the properties of the hole polaron are properly captured by our computational approach. In contrast, the position of the conduction band-edge states is noticeably influenced by SOC. [7, 10] However, previous studies have shown that the introduction of SOC have negligible effects on polaron localization[4] and on the calculated stabilization energies.[60] Therefore, the present estimate of the hopping barrier, based on total-energy differences, should only be marginally affected by the SOC effects.

The calculated energy barriers can then be used to estimate the thermally activated hopping rate (k_{hop}) from transition-state theory:

$$k_{\mathrm{hop}} = Ae^{-\frac{\Delta E}{k_B T}}$$

where ΔE is the calculated energy barrier and A can be defined as a frequency of the phonons involved in the charge transfer process. If we consider an upper bound for $A = \nu_{\mathrm{Pb-I}}$ *i.e.* the stretching frequency of Pb-I bonds in $CH_3NH_3PbI_3$ ($\sim$100 cm^{-1} from previous studies[37, 61-63]) we estimate hopping frequencies $k \sim 10^{-10}\ s^{-1}$ and $\sim 10^{-11}\ s^{-1}$ for hole and electron polarons, respectively. This corresponds to sub-nanosecond dynamics, up to 2-3 orders of magnitude slower than the sub-picosecond hopping time-scale observed in MD simulations.[4, 38] This discrepancy clearly indicate that the rearrangement of the Pb-I sub-lattice alone cannot explain the dynamics of polaron hopping in $CH_3NH_3PbI_3$. To get further insight, we recalculate the energy barriers along the same hopping pathway but removing the organic cations from the simulation. In these calculations, the total charge of the supercell is determined by the number of missing cations but we still keep a hole (electron) in the valence (conduction) band edge. The results collected in Fig. 3 (dashed lines) illustrate an inversion of the energy barrier for both hole and electron polarons: the polaronic states are now found to be at higher energy with respect to the semi-localized states pertaining to the intermediate models. The inverted barrier for the hole polaron is somewhat smaller (90±10 meV), in absolute terms, than that calculated for the original system containing methylammonium cations, while for the electron polaron it is slightly larger. This can be associated to the larger distortions in the Pb-I framework observed for the electron polaron.[4] Overall, these results show that polaronic structures are only favourable when the distortion in the inorganic lattice is coupled to the dipole field generated by the A-site cations. Therefore, the inorganic sub-lattice would rather support delocalized electronic states, in line with common inorganic semiconductors such as GaAs, but charge localization is essentially enforced by the A-site cations. Furthermore, from this analysis, the hopping appears to be related to the rearrangement of the organic cations. In this framework, at room temperature fluctuations of the dipole field attained on very short time-scales can induce the migration of the polaron in a different part of the inorganic sub-lattice. The latter, being soft, is also

significantly subject to thermal disorder and hence can easily localize again the charge in the region "indicated" by the instantaneous orientation of the organic cations.

In order to confirm the origin of the fast polaron hopping, we perform an *ab initio* MD simulation in presence of an extra positive charge of a modified $CH_3NH_3PbI_3$ in which the mass of the hydrogen atoms has been increased twelvefold. In this way, $CH_3NH_3^+$ cations are noticeably weighted down, thus possibly affecting the amplitude and the frequency of the fluctuations, which we indicate to be responsible of polaron formation and hopping. The MD simulation is carried out in the *NVT* ensemble, the target temperature is set to 300 K and is controlled by a Nosé-Hoover thermostat.[66, 67] A time step of 0.5 femtoseconds is employed and the MD is carried out for 5 ps.

The starting configuration of the simulation is model **1**, for which no hole polaron has been observed upon relaxation, because of the absence of a net dipole field. The same model was found to form polarons in less than 1 ps of MD.[4] Furthermore, the polarons have found to hop frequently from one localization plane to another [e.g. the hole polaron in Fig. 4(a)]. At variance with that, the hole polaron is formed only after two picoseconds of MD for the "heavy" $CH_3NH_3PbI_3$ system. Furthermore, the hole is remarkably less mobile, as it remains localized on the same Pb-I plane orthogonal to the tetragonal axis throughout the rest of the simulation with only a few cases in which the charge is shared with an adjacent plane [cf. Fig. 4 (b)]. To rationalize these results, we analyse the distribution of the orientations of $CH_3NH_3^+$ cations for the regular and "heavy" $CH_3NH_3PbI_3$. In particular, we consider (i) the angle ϕ formed by the CN axis with the *ab* plane and thus representing the tilting of the molecule with respect to the *c* axis and (ii) the angle θ between the projection of the CN axis on the *ab* plane and the *a* axis. For structural model **1** the average value of ϕ and θ is 180° and 0°, respectively, since the orientation of the cations is alternated (cf. Fig. 1). Distributions of the average values of ϕ and θ during the MD provides information on the dipole field induced by the organic cations and on its variations. Figures 4 (c) and (d) clearly illustrate larger changes in the dipole field for regular $CH_3NH_3PbI_3$, as broader distributions are

observed for both ϕ and θ. In contrast, the "heavy" $CH_3NH_3PbI_3$ features only exiguous changes in ϕ and θ along the MD trajectory (cf. SI for time-evolution of the orientation for a selected $CH_3NH_3^+$), a consequence of the increased weight of the methylammonium cation. This in turn slows down both polaron formation and hopping, as rearrangements of organic dipoles favouring charge localization and hopping are more difficult to attain when the rotational and vibrational modes or $CH_3NH_3^+$ are damped.

The present results also allow us to rationalize the observed correlation between diffusion lengths and rotation times of cations. In particular, longer diffusion lengths have been measured for $CH(NH_2)_2PbI_3$,[32] a material for which polaron formation has also been predicted.[60] In fact, the formamidinium cation is less polar and forms weaker hydrogen bonds. This allows for faster fluctuations [cf. SI for a comparison between $CH_3NH_3^+$ and $CH(NH_2)^+$] which may favour the separation of the charge carriers and enhance their diffusion length, as experimentally observed.[32, 40] Furthermore, we notice that polaron formation has also been observed for fully inorganic perovskites, such as $CsPbI_3$.[29, 60] For this system, the measured polaron formation time is more than doubled compared to that of $CH_3NH_3PbI_3$ [28] In this case, the field-induced charge separation is given by the displacement of the Cs^+ ions, which is much slower than the rotation and the libration of organic cations. Overall, the random motion of the A-site cations explains both (i) the occurrence of polaronic energy levels inside the band gap of lead iodide perovskites and (ii) the hopping of polarons from one site to another through a semi-localized state. Finally, it should be noted that organic cations themselves appear to be only marginally affected by the presence of extra charges[4] and by the application of an external electric field.[64, 65] Therefore, *hopping can be fast but still random* as the motion of the cations which promote it, thus qualitatively explaining the measured low mobility of charge carriers observed for lead halide perovskites. We note that, while a band conduction model might be also invoked to explain charge diffusion, it would however ignore the polaronic nature of charge carriers which has been experimentally demonstrated and would not provide an interpretation of the measured low mobility.

In conclusion, we studied the electronic structure of polarons in different structural models of tetragonal $CH_3NH_3PbI_3$. Our results allow us to determine the origin of both charge localization and stabilization in this material. While the former was found to be induced by the dipole field generated by the organic cations, only rearrangements in the inorganic sub-lattice provide the energetic stabilization to form polarons. Based on the same models, we studied the mechanism of polaron hopping and calculated the hopping energy barriers of 150 and 80 meV for hole and electron polarons, respectively. These values are consistent with the calculated stabilization energy for the respective models, in accord with the semi-localized nature of the charges at the transition state. Analysis of the energy barriers reveals that these arise mainly from the rearrangement of the organic cations. This allows us to explain the observed correlation between diffusion lengths and rotation times of cations, as faster cations enable a more rapid change of the dipole field associated to the hopping. Furthermore, the low mobility of charge carriers observed in experiments is connected the non-directional nature of polaron hopping, due to the random motion of the organic cations.

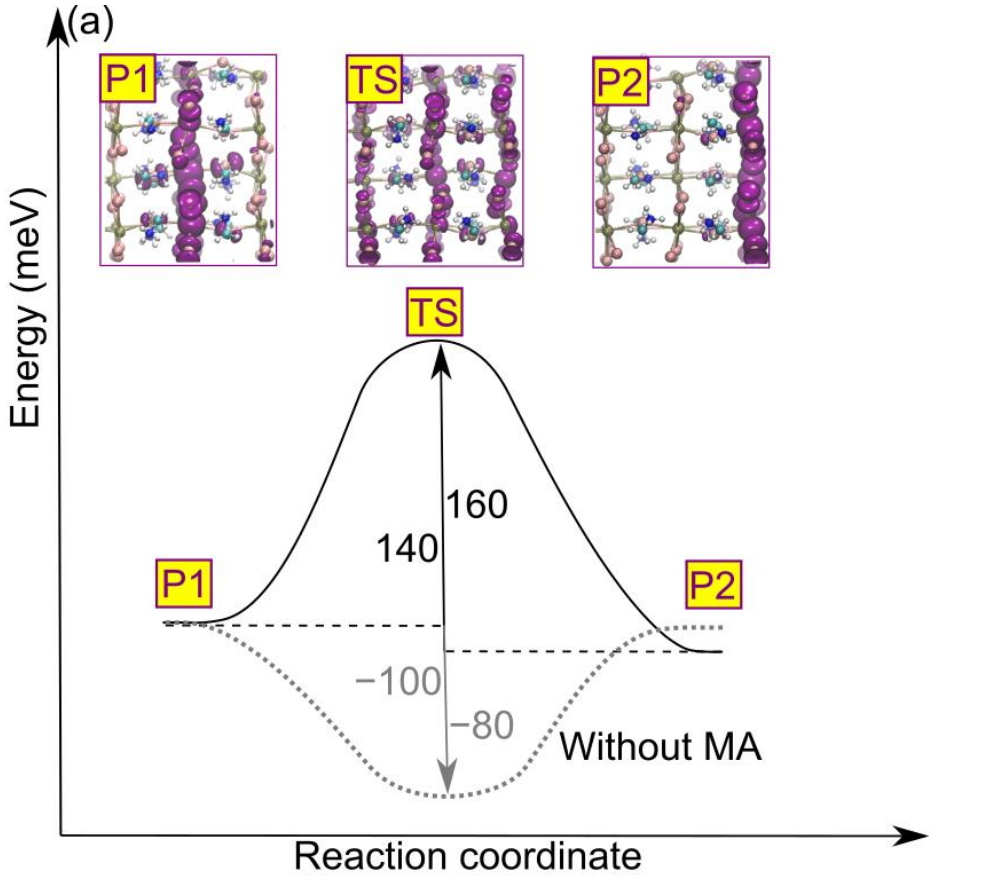
(a)
P1
TS
P2
Energy (meV)
TS
160
140
P1
P2
−100
−80
Without MA
Reaction coordinate

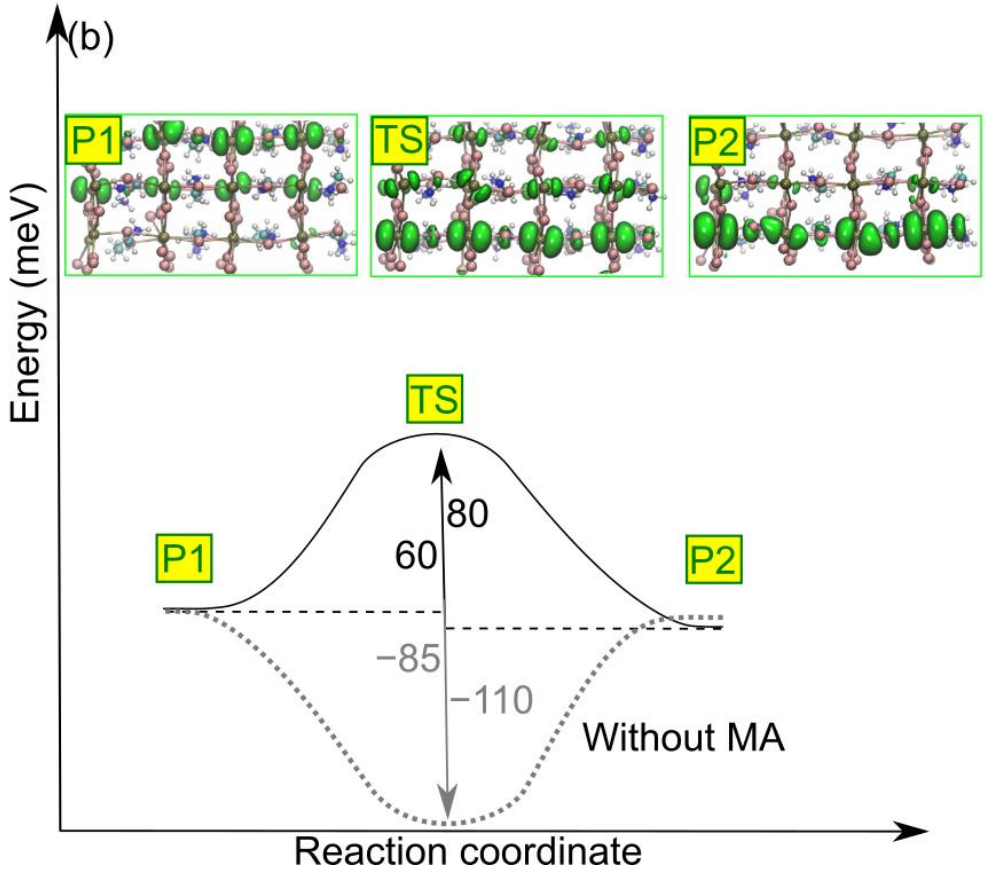
(b)
P1
TS
P2
Energy (meV)
TS
80
60
P1
P2
−85
−110
Without MA
Reaction coordinate

Figure 3. Reaction energy profile illustrating (a) the hole diffusion through adjacent Pb-I planes and (b) the electron diffusion through adjacent Pb-I chains of atoms. Isodensity representations of the wavefunctions are given for the polaronic structures (P1 and P2) and for the transition state (TS). Dotted grey lines represent the energy diagrams achieved from calculations in which the methylammonium cations have been removed (cf. main text).

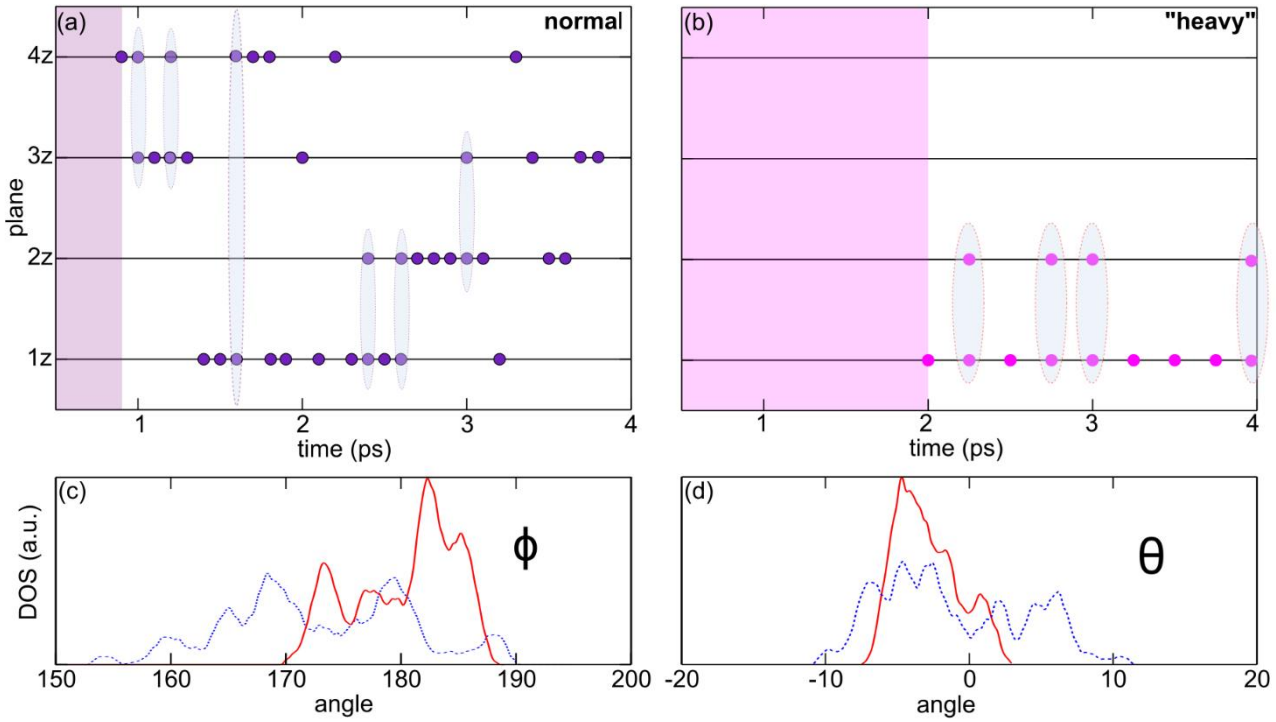

Figure 4. Hopping of the charge localization during the molecular dynamics of the extra hole for regular (a) and "heavy" (b) $CH_3NH_3PbI_3$. The hole density localizes in planes of the inorganic sub-lattice orthogonal to the tetragonal axis (labeled 1z to 4z). Cyan circles highlight configurations in which the hole is shared among adjacent planes. Distribution of the average ϕ and θ angles for regular (blue dotted lines) and "heavy" (red solid lines) $CH_3NH_3PbI_3$ are given in panel (c) and (d), respectively.

Associated content

Supporting Information

Calculation of the polaron binding energy as a function of the fraction of Fock exchange introduced in the hybrid functional, an analysis of results achieved with different supercell sizes and shapes, a detailed explanation of the linear transit method and a comparison with energy barriers calculated with the nudge elastic band method, time-evolution of ϕ angle for regular and "heavy" $CH_3NH_3PbI_3$, time-evolution of ϕ and θ angles for $CH_3NH_3^+$ in $CH_3NH_3PbI_3$ and of $CH(NH_2)_2^+$ in $CH(NH_2)_2PbI_3$, and additional Refs. 68-76.

Acknowledgment:
This project has received funding from the European Union's Horizon 2020 research and innovation programme under grant agreement No 764047 of the ESPRESSO project. The Ministero dell'Istruzione dell'Università e della Ricerca (MIUR) and Università degli Studi di Perugia are acknowledged for financial support through the program "Dipartimenti di Eccellenza 2018-2022" (Grant AMIS) to F.D.A.

References

1. Etgar, L.; Gao, P.; Xue, Z.; Peng, Q.; Chandiran, A. K.; Liu, B.; Nazeeruddin, M. K.; Grätzel, M., Mesoscopic CH3NH3PbI3/TiO2 Heterojunction Solar Cells. *Journal of the American Chemical Society* **2012,** *134* (42), 17396-17399.

2. Burschka, J.; Pellet, N.; Moon, S.-J.; Humphry-Baker, R.; Gao, P.; Nazeeruddin, M. K.; Grätzel, M., Sequential Deposition as a Route to High-Performance Perovskite-Sensitized Solar Cells. *Nature* **2013,** *499*, 316.

3. Brenner, T. M.; Egger, D. A.; Kronik, L.; Hodes, G.; Cahen, D., Hybrid Organic—Inorganic Perovskites: Low-Cost Semiconductors with Intriguing Charge-Transport Properties. *Nature Reviews Materials* **2016,** *1*, 15007.

4. Ambrosio, F.; Wiktor, J.; De Angelis, F.; Pasquarello, A., Origin of Low Electron–Hole Recombination Rate in Metal Halide Perovskites. *Energy & Environmental Science* **2018,** *11* (1), 101-105.

5. Chiarella, F.; Zappettini, A.; Licci, F.; Borriello, I.; Cantele, G.; Ninno, D.; Cassinese, A.; Vaglio, R., Combined Experimental and Theoretical Investigation of Optical, Structural, and Electronic Properties of $CH_3NH_3SnX_3$ Thin Films (X=Cl, Br). *Physical Review B* **2008,** *77* (4), 045129.

6. Stoumpos, C. C.; Malliakas, C. D.; Kanatzidis, M. G., Semiconducting Tin and Lead Iodide Perovskites with Organic Cations: Phase Transitions, High Mobilities, and Near-Infrared Photoluminescent Properties. *Inorganic Chemistry* **2013,** *52* (15), 9019-9038.

7. Even, J.; Pedesseau, L.; Jancu, J.-M.; Katan, C., Importance of Spin–Orbit Coupling in Hybrid Organic/Inorganic Perovskites for Photovoltaic Applications. *The Journal of Physical Chemistry Letters* **2013,** *4* (17), 2999-3005.

8. Ogomi, Y.; Morita, A.; Tsukamoto, S.; Saitho, T.; Fujikawa, N.; Shen, Q.; Toyoda, T.; Yoshino, K.; Pandey, S. S.; Ma, T.; Hayase, S., CH3NH3SnxPb(1–x)I3 Perovskite Solar Cells Covering up to 1060 nm. *The Journal of Physical Chemistry Letters* **2014,** *5* (6), 1004-1011.

9. Eperon, G. E.; Stranks, S. D.; Menelaou, C.; Johnston, M. B.; Herz, L. M.; Snaith, H. J., Formamidinium Lead Trihalide: a Broadly Tunable Perovskite for Efficient Planar Heterojunction Solar Cells. *Energy & Environmental Science* **2014,** *7* (3), 982-988.

10. Umari, P.; Mosconi, E.; De Angelis, F., Relativistic GW Calculations on $CH_3NH_3PbI_3$ and $CH_3NH_3SnI_3$ Perovskites for Solar Cell Applications. *Scientific Reports* **2014,** *4*, 4467.

11. Ponseca, C. S.; Savenije, T. J.; Abdellah, M.; Zheng, K.; Yartsev, A.; Pascher, T.; Harlang, T.; Chabera, P.; Pullerits, T.; Stepanov, A.; Wolf, J.-P.; Sundström, V., Organometal Halide Perovskite Solar Cell Materials Rationalized: Ultrafast Charge Generation, High and Microsecond-Long Balanced Mobilities, and Slow Recombination. *Journal of the American Chemical Society* **2014,** *136* (14), 5189-5192.

12. Edri, E., E. Edri, S. Kirmayer, S. Mukhopadhyay, K. Gartsman, G. Hodes, and D. Cahen, Elucidating the Charge Carrier Separation and Working Mechanism of $CH_3NH_3PbI_{3-x}Cl_x$ Perovskite Solar Cells. *Nature Communications* **2014,** *5*, 3461.

13. Hutter, E. M.; Gélvez-Rueda, M. C.; Osherov, A.; Bulović, V.; Grozema, F. C.; Stranks, S. D.; Savenije, T. J., Direct–Indirect Character of the Bandgap in Methylammonium Lead Iodide Perovskite. *Nature Materials* **2016,** *16*, 115.

14. Crothers, T. W.; Milot, R. L.; Patel, J. B.; Parrott, E. S.; Schlipf, J.; Müller-Buschbaum, P.; Johnston, M. B.; Herz, L. M., Photon Reabsorption Masks Intrinsic Bimolecular Charge-Carrier Recombination in $CH_3NH_3PbI_3$ Perovskite. *Nano Letters* **2017,** *17* (9), 5782-5789.

15. Stranks, S. D.; Eperon, G. E.; Grancini, G.; Menelaou, C.; Alcocer, M. J. P.; Leijtens, T.; Herz, L. M.; Petrozza, A.; Snaith, H. J., Electron-Hole Diffusion Lengths Exceeding 1 Micrometer in an Organometal Trihalide Perovskite Absorber. *Science* **2013,** *342* (6156), 341-344.

16. Li, D.; Liao, P.; Shai, X.; Huang, W.; Liu, S.; Li, H.; Shen, Y.; Wang, M., Recent Progress on Stability Issues of Organic–Inorganic Hybrid Lead Perovskite-based Solar Cells. *RSC Advances* **2016,** *6* (92), 89356-89366.

17. Sell, D. D.; Jr., H. C. C., Optical Absorption and Photoluminescence Studies of Thin GaAs Layers in GaAs–$Al_xGa_{1-x}As$ double heterostructures. *Journal of Applied Physics* **1974,** *45* (2), 800-807.

18. Brenner, T. M.; Egger, D. A.; Rappe, A. M.; Kronik, L.; Hodes, G.; Cahen, D., Are Mobilities in Hybrid Organic–Inorganic Halide Perovskites Actually "High"? *The Journal of Physical Chemistry Letters* **2015,** *6* (23), 4754-4757.

19. Ma, J.; Wang, L.-W., Nanoscale Charge Localization Induced by Random Orientations of Organic Molecules in Hybrid Perovskite CH3NH3PbI3. *Nano Letters* **2015,** *15* (1), 248-253.

20. Quarti, C.; Mosconi, E.; De Angelis, F., Structural and Electronic Properties of Organo-Halide Hybrid Perovskites From ab initio Molecular Dynamics. *Physical Chemistry Chemical Physics* **2015,** *17* (14), 9394-9409.

21. Frost, J. M.; Butler, K. T.; Brivio, F.; Hendon, C. H.; van Schilfgaarde, M.; Walsh, A., Atomistic Origins of High-Performance in Hybrid Halide Perovskite Solar Cells. *Nano Letters* **2014,** *14* (5), 2584-2590.

22. Even, J.; Pedesseau, L.; Katan, C., Analysis of Multivalley and Multibandgap Absorption and Enhancement of Free Carriers Related to Exciton Screening in Hybrid Perovskites. *The Journal of Physical Chemistry C* **2014,** *118* (22), 11566-11572.

23. Chen, Y.; Yi, H. T.; Wu, X.; Haroldson, R.; Gartstein, Y. N.; Rodionov, Y. I.; Tikhonov, K. S.; Zakhidov, A.; Zhu, X. Y.; Podzorov, V., Extended Carrier Lifetimes and Diffusion in Hybrid Perovskites Revealed by Hall Effect and Photoconductivity Measurements. *Nature Communications* **2016,** *7*, 12253.

24. Johnston, M. B.; Herz, L. M., Hybrid Perovskites for Photovoltaics: Charge-Carrier Recombination, Diffusion, and Radiative Efficiencies. *Accounts of Chemical Research* **2016,** *49* (1), 146-154.

25. Bokdam, M.; Sander, T.; Stroppa, A.; Picozzi, S.; Sarma, D. D.; Franchini, C.; Kresse, G., Role of Polar Phonons in the Photo Excited State of Metal Halide Perovskites. *Scientific Reports* **2016,** *6*, 28618.

26. Wehrenfennig, C.; Eperon, G. E.; Johnston, M. B.; Snaith, H. J.; Herz, L. M., High Charge Carrier Mobilities and Lifetimes in Organolead Trihalide Perovskites. *Advanced materials* **2014,** *26* (10), 1584-1589.

27. Zhu, X. Y.; Podzorov, V., Charge Carriers in Hybrid Organic–Inorganic Lead Halide Perovskites Might Be Protected as Large Polarons. *The Journal of Physical Chemistry Letters* **2015,** *6* (23), 4758-4761.

28. Zhu, H.; Miyata, K.; Fu, Y.; Wang, J.; Joshi, P. P.; Niesner, D.; Williams, K. W.; Jin, S.; Zhu, X.-Y., Screening in Crystalline Liquids Protects Energetic Carriers in Hybrid Perovskites. *Science* **2016,** *353* (6306), 1409-1413.

29. Miyata, K.; Meggiolaro, D.; Trinh, M. T.; Joshi, P. P.; Mosconi, E.; Jones, S. C.; De Angelis, F.; Zhu, X.-Y., Large Polarons in Lead Halide Perovskites. *Science Advances* **2017,** *3* (8), e1701217.

30. Bretschneider, S. A.; Ivanov, I.; Wang, H. I.; Miyata, K.; Zhu, X.; Bonn, M., Quantifying Polaron Formation and Charge Carrier Cooling in Lead-Iodide Perovskites. *Advanced Materials* **2018,** *30* (29), 1707312.

31. Chen, T.; Foley, B. J.; Ipek, B.; Tyagi, M.; Copley, J. R. D.; Brown, C. M.; Choi, J. J.; Lee, S.-H., Rotational Dynamics of Organic Cations in the $CH_3NH_3PbI_3$ Perovskite. *Physical Chemistry Chemical Physics* **2015,** *17* (46), 31278-31286.

32. Kubicki, D. J.; Prochowicz, D.; Hofstetter, A.; Péchy, P.; Zakeeruddin, S. M.; Grätzel, M.; Emsley, L., Cation Dynamics in Mixed-Cation $(MA)_x(FA)_{1-x}PbI_3$ Hybrid Perovskites from Solid-State NMR. *Journal of the American Chemical Society* **2017,** *139* (29), 10055-10061.

33. Dastidar, S.; Li, S.; Smolin, S. Y.; Baxter, J. B.; Fafarman, A. T., Slow Electron–Hole Recombination in Lead Iodide Perovskites Does Not Require a Molecular Dipole. *ACS Energy Letters* **2017,** *2* (10), 2239-2244.

34. Carignano, M. A.; Aravindh, S. A.; Roqan, I. S.; Even, J.; Katan, C., Critical Fluctuations and Anharmonicity in Lead Iodide Perovskites from Molecular Dynamics Supercell Simulations. *The Journal of Physical Chemistry C* **2017,** *121* (38), 20729-20738.

35. Marronnier, A.; Roma, G.; Carignano, M. A.; Bonnassieux, Y.; Katan, C.; Even, J.; Mosconi, E.; De Angelis, F., Influence of Disorder and Anharmonic Fluctuations on the Dynamical Rashba Effect in Purely Inorganic Lead-Halide Perovskites. *The Journal of Physical Chemistry C* **2019,** *123* (1), 291-298.

36. Filippetti, A.; Delugas, P.; Mattoni, A., Radiative Recombination and Photoconversion of Methylammonium Lead Iodide Perovskite by First Principles: Properties of an Inorganic Semiconductor within a Hybrid Body. *The Journal of Physical Chemistry C* **2014,** *118* (43), 24843-24853.

37. Wright, A. D.; Verdi, C.; Milot, R. L.; Eperon, G. E.; Pérez-Osorio, M. A.; Snaith, H. J.; Giustino, F.; Johnston, M. B.; Herz, L. M., Electron–Phonon Coupling in Hybrid Lead Halide Perovskites. *Nature Communications* **2016,** *7*, 11755.

38. Wiktor, J.; Ambrosio, F.; Pasquarello, A., Mechanism Suppressing Charge Recombination at Iodine Defects in $CH_3NH_3PbI_3$ by polaron formation. *Journal of Materials Chemistry A* **2018,** *6* (35), 16863-16867.

39. Uratani, H.; Yamashita, K., Inorganic Lattice Fluctuation Induces Charge Separation in Lead Iodide Perovskites: Theoretical Insights. *The Journal of Physical Chemistry C* **2017,** *121* (48), 26648-26654.

40. Gong, J.; Yang, M.; Ma, X.; Schaller, R. D.; Liu, G.; Kong, L.; Yang, Y.; Beard, M. C.; Lesslie, M.; Dai, Y.; Huang, B.; Zhu, K.; Xu, T., Electron–Rotor Interaction in Organic–Inorganic Lead Iodide Perovskites Discovered by Isotope Effects. *The Journal of Physical Chemistry Letters* **2016,** *7* (15), 2879-2887.

41. Zheng, F.; Wang, L.-w., Large Polaron Formation and its Effect on Electron Transport in Hybrid Perovskites. *Energy & Environmental Science* **2019,** 12, 1219-1230.

42. Poncé, S.; Schlipf, M.; Giustino, F., Origin of Low Carrier Mobilities in Halide Perovskites. *ACS Energy Letters* **2019,** *4* (2), 456-463.

43. Zheng, K.; Abdellah, M.; Zhu, Q.; Kong, Q.; Jennings, G.; Kurtz, C. A.; Messing, M. E.; Niu, Y.; Gosztola, D. J.; Al-Marri, M. J.; Zhang, X.; Pullerits, T.; Canton, S. E., Direct Experimental Evidence for Photoinduced Strong-Coupling Polarons in Organolead Halide Perovskite Nanoparticles. *The Journal of Physical Chemistry Letters* **2016,** *7* (22), 4535-4539.

44. Perdew, J. P.; Ernzerhof, M.; Burke, K., Rationale for Mixing Exact Exchange with Density Functional Approximations. *The Journal of chemical physics* **1996,** *105* (22), 9982-9985.

45. Adamo, C.; Barone, V., Toward Reliable Density Functional Methods without Adjustable Parameters: The PBE0 Model. *The Journal of chemical physics* **1999,** *110* (13), 6158-6170.

46. Perdew, J. P.; Parr, R. G.; Levy, M.; Balduz, J. L., Density-Functional Theory for Fractional Particle Number: Derivative Discontinuities of the Energy. *Physical Review Letters* **1982,** *49* (23), 1691-1694.

47. Miceli, G.; Chen, W.; Reshetnyak, I.; Pasquarello, A., Nonempirical Hybrid Functionals for Band Gaps and Polaronic Distortions in Solids. *Physical Review B* **2018,** *97* (12), 121112.

48. Nguyen, N. L.; Colonna, N.; Ferretti, A.; Marzari, N., Koopmans-Compliant Spectral Functionals for Extended Systems. *Physical Review X* **2018,** *8* (2), 021051.

49. Vydrov, O. A.; Van Voorhis, T., Nonlocal van der Waals Density Functional: The Simpler the Better. *The Journal of chemical physics* **2010,** *133* (24), 244103.

50. Sabatini, R.; Gorni, T.; De Gironcoli, S., Nonlocal van der Waals Density Functional Made Simple and Efficient. *Physical Review B* **2013,** *87* (4), 041108.

51. VandeVondele, J.; Krack, M.; Mohamed, F.; Parrinello, M.; Chassaing, T.; Hutter, J., Quickstep: Fast and Accurate Density Functional Calculations Using a Mixed Gaussian and Plane Waves Approach. *Computer Physics Communications* **2005,** *167* (2), 103-128.

52. Goedecker, S.; Teter, M.; Hutter, J., Separable Dual-Space Gaussian Pseudopotentials. *Physical Review B* **1996,** *54* (3), 1703.

53. VandeVondele, J.; Hutter, J., Gaussian Basis Sets for Accurate Calculations on Molecular systems in gas and condensed phases. *The Journal of Chemical Physics* **2007,** *127* (11), 114105.

54. Guidon, M.; Hutter, J.; VandeVondele, J., Auxiliary Density Matrix Methods for Hartree−Fock Exchange Calculations. *Journal of Chemical Theory and Computation* **2010,** *6* (8), 2348-2364.

55. Kawamura, Y.; Mashiyama, H.; Hasebe, K., Structural Study on Cubic–Tetragonal Transition of CH3NH3PbI3. *Journal of the Physical Society of Japan* **2002,** *71* (7), 1694-1697.

56. Lin, Q.; Armin, A.; Nagiri, R. C. R.; Burn, P. L.; Meredith, P., Electro-Optics of Perovskite Solar Cells. *Nature Photonics* **2014,** *9*, 106.

57. Quarti, C.; Mosconi, E.; De Angelis, F., Interplay of Orientational Order and Electronic Structure in Methylammonium Lead Iodide: Implications for Solar Cell Operation. *Chemistry of Materials* **2014,** *26* (22), 6557-6569.

58. Halgren, T. A.; Lipscomb, W. N., The Synchronous-Transit Method for Determining Reaction Pathways and Locating Molecular Transition States. *Chemical Physics Letters* **1977,** *49* (2), 225-232.

59. Meggiolaro, D.; De Angelis, F., First-Principles Modeling of Defects in Lead Halide Perovskites: Best Practices and Open Issues. *ACS Energy Letters* **2018,** *3* (9), 2206-2222.

60. Mahata, A.; Meggiolaro, D.; De Angelis, F., From Large to Small Polarons in Lead, Tin, and Mixed Lead–Tin Halide Perovskites. *The Journal of Physical Chemistry Letters* **2019,** *10* (8), 1790-1798.

61. Quarti, C.; Grancini, G.; Mosconi, E.; Bruno, P.; Ball, J. M.; Lee, M. M.; Snaith, H. J.; Petrozza, A.; De Angelis, F., The Raman Spectrum of the $CH_3NH_3PbI_3$ Hybrid Perovskite: Interplay of Theory and Experiment. *The Journal of Physical Chemistry Letters* **2014,** *5* (2), 279-284.

62. Leguy, A. M. A.; Goñi, A. R.; Frost, J. M.; Skelton, J.; Brivio, F.; Rodríguez-Martínez, X.; Weber, O. J.; Pallipurath, A.; Alonso, M. I.; Campoy-Quiles, M.; Weller, M. T.; Nelson, J.; Walsh, A.; Barnes, P. R. F., Dynamic Disorder, Phonon Lifetimes, and the Assignment of Modes to the Vibrational Spectra of Methylammonium Lead Halide Perovskites. *Physical Chemistry Chemical Physics* **2016,** *18* (39), 27051-27066.

63. Brivio, F.; Frost, J. M.; Skelton, J. M.; Jackson, A. J.; Weber, O. J.; Weller, M. T.; Goñi, A. R.; Leguy, A. M. A.; Barnes, P. R. F.; Walsh, A., Lattice Dynamics and Vibrational Spectra of the Orthorhombic, Tetragonal, and Cubic Phases of Methylammonium Lead Iodide. *Physical Review B* **2015,** *92* (14), 144308.

64. Liu, S.; Cohen, R. E., Response of Methylammonium Lead Iodide to External Stimuli and Caloric Effects from Molecular Dynamics Simulations. *The Journal of Physical Chemistry C* **2016,** *120* (31), 17274-17281.

65. Chen, B.; Li, T.; Dong, Q.; Mosconi, E.; Song, J.; Chen, Z.; Deng, Y.; Liu, Y.; Ducharme, S.; Gruverman, A.; Angelis, F. D.; Huang, J., Large Electrostrictive Response in Lead Halide Perovskites. *Nature Materials* **2018,** *17* (11), 1020-1026.

66. Nosé, S., A unified formulation of the constant temperature molecular dynamics methods. *The Journal of Chemical Physics* **1984,** *81* (1), 511-519.

67. Hoover, W. G., Canonical dynamics: Equilibrium phase-space distributions. *Physical Review A* **1985,** *31* (3), 1695-1697.

68. Komsa, H.-P.; Rantala, T. T.; Pasquarello, A., Finite-Size Supercell Correction Schemes for Charged Defect Calculations. *Physical Review B* **2012,** *86* (4), 045112.

69. Freysoldt, C.; Grabowski, B.; Hickel, T.; Neugebauer, J.; Kresse, G.; Janotti, A.; Van de Walle, C. G., First-Principles Calculations for Point Defects in Solids. *Reviews of Modern Physics* **2014,** *86* (1), 253-305.

70. Freysoldt, C.; Neugebauer, J.; Van de Walle, C. G., Fully Ab Initio Finite-Size Corrections for Charged-Defect Supercell Calculations. *Physical Review Letters* **2009,** *102* (1), 016402.

71. Alkauskas, A.; Broqvist, P.; Pasquarello, A., Defect Energy Levels in Density Functional Calculations: Alignment and Band Gap Problem. *Physical Review Letters* **2008,** *101* (4), 046405.

72. Alkauskas, A.; Broqvist, P.; Pasquarello, A., Defect Levels Through Hybrid Density Functionals: Insights and Applications. *Physica Status Solidi (b)* **2011,** *248* (4), 775-789.

73. Komsa, H.-P.; Broqvist, P.; Pasquarello, A., Alignment of Defect Levels and Band Edges through Hybrid Functionals: Effect of Screening in the Exchange Term. *Physical Review B* **2010,** *81* (20), 205118.

74. Ambrosio, F.; Miceli, G.; Pasquarello, A., Redox Levels in Aqueous Solution: Effect of van der Waals Interactions and Hybrid Functionals. *The Journal of Chemical Physics* **2015,** *143* (24), 244508.

75. Alkauskas, A.; Broqvist, P.; Devynck, F.; Pasquarello, A., Band Offsets at Semiconductor-Oxide Interfaces from Hybrid Density-Functional Calculations. *Physical Review Letters* **2008,** *101* (10), 106802.

76. Henkelman, G.; Jónsson, H., Improved Tangent Estimate in the Nudged Elastic Band Method for Finding Minimum Energy Paths and Saddle Points. *The Journal of Chemical Physics* **2000,** *113* (22), 9978-9985.